NASA TECHNICAL NOTE

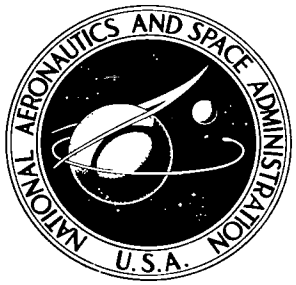

NASA TN D-5907

NASA TN D-5907

AN INVERSE-METHOD SOLUTION FOR RADIATING, NONADIABATIC, EQUILIBRIUM INVISCID FLOW OVER A BLUNT BODY

by Ralph A. Falanga and Edward M. Sullivan

Langley Research Center

Hampton, Va. 23365

NATIONAL AERONAUTICS AND SPACE ADMINISTRATION • WASHINGTON, D. C. • AUGUST 1970

1. Report No.	2. Government Accession No.	3. Recipient's Catalog No.
NASA TN D-5907		

4. Title and Subtitle	5. Report Date
AN INVERSE-METHOD SOLUTION FOR RADIATING, NONADIABATIC, EQUILIBRIUM INVISCID FLOW OVER A BLUNT BODY	August 1970
	6. Performing Organization Code
7. Author(s)	8. Performing Organization Report No.
Ralph A. Falanga and Edward M. Sullivan	L-7209
	10. Work Unit No.
9. Performing Organization Name and Address	124-07-18-01
NASA Langley Research Center Hampton, Va. 23365	11. Contract or Grant No.
	13. Type of Report and Period Covered
12. Sponsoring Agency Name and Address	Technical Note
National Aeronautics and Space Administration Washington, D.C. 20546	14. Sponsoring Agency Code

15. Supplementary Notes

16. Abstract

An inverse flow-field program capable of making calculations with an equilibrium air gas model and a realistic radiation model has been developed. The program is capable of calculating the inviscid flow field on a blunt body over a large range of conditions. The primary restrictions are that the assumed shock be analytic in shape and that the postshock temperature be between 10 000° K and 15 000° K.

Comparisons are presented which show substantial agreement between the results from the present program, results from a direct-method program, and results from a time-asymptotic-method program for a nonadiabatic flow field. The inverse method can be operated with 8 to 24 rays and 5, 7, 9, or 11 radiative-flux calculations along each ray. A brief study has shown that a nominal set of 14 rays and 9 radiative flux calculations will produce accurate results over the entire range of applicability of the program.

17. Key Words (Suggested by Author(s))	18. Distribution Statement
Numerical flow-field solutions, coupled radiation Inverse method	Unclassified – Unlimited

19. Security Classif. (of this report)	20. Security Classif. (of this page)	21. No. of Pages	22. Price*
Unclassified	Unclassified	34	$3.00

*For sale by the Clearinghouse for Federal Scientific and Technical Information
Springfield, Virginia 22151

AN INVERSE-METHOD SOLUTION FOR RADIATING, NONADIABATIC, EQUILIBRIUM INVISCID FLOW OVER A BLUNT BODY

By Ralph A. Falanga and Edward M. Sullivan
Langley Research Center

SUMMARY

An inverse flow-field program capable of making calculations with an equilibrium air gas model and a realistic radiation model has been developed. The program is capable of calculating the inviscid flow field on a blunt body over a large range of conditions. The primary restrictions are that the assumed shock be analytic in shape and that the postshock temperature be between 10 000° K and 15 000° K.

Comparisons are presented which show substantial agreement between the results from the present program, results from a direct-method program, and results from a time-asymptotic-method program for a nonadiabatic flow field. The inverse method can be operated with 8 to 24 rays and 5, 7, 9, or 11 radiative-flux calculations along each ray. A brief study has shown that a nominal set of 14 rays and 9 radiative flux calculations will produce accurate results over the entire range of applicability of the program.

INTRODUCTION

In the past several years a great deal of effort has gone into the development of computer programs which could be used to analyze the flow in the subsonic region behind the bow shock on a blunt body at hypersonic speeds. The early work in this area has been well documented, and the fundamentals can be found in a standard text such as that of Hayes and Probstein (ref. 1). In particular, three techniques have been developed and used extensively. The techniques, with an example of a working program for each, are: the direct method (Garrett, Suttles, and Perkins, ref. 2), the time-dependent method (Moretti and Abbett, ref. 3), and the inverse method (Lomax and Inouye, ref. 4). The solutions presented in these references are for inviscid adiabatic flows. (Ref. 2 carries a radiative flux term through the program development but never uses it in the calculations.)

More recent work has been aimed at exploring the problems associated with entry velocities (10 km/sec or higher) at which the nonadiabatic effects become important. For stagnation-region calculations, a large number of specialized solutions have been developed. In terms of the basic techniques mentioned previously, nonadiabatic effects have

been included in the direct method by the work of Suttles (ref. 5) and in the time-dependent method by the work of Callis (ref. 6). The inverse method has not been as well developed. Cheng and Vincenti (ref. 7) used the classical inverse method to study radiation effects on various flow-field parameters. The analysis was, however, simplified by the assumptions of a perfect gas with a gray-gas radiation model. Olstad (ref. 8) used the simplified inverse method of Maslen (ref. 9) and an approximate nongray radiation model for equilibrium air.

The present report presents the results of an effort to develop an inverse flow-field program which eliminates the approximations mentioned. The solution technique is the classical inverse technique described in reference 1. The gas model is equilibrium air, and the radiation model is the reasonably detailed model of reference 10, the same model as used in reference 5. This effort was undertaken primarily to provide solutions which could be used to test the validity of the more approximate programs, such as that of reference 5. The authors believe, however, that the effort was justified in its own right to fill the obvious gap in the inverse-program development.

SYMBOLS

Primed symbols (') indicate dimensional quantities. Since it is convenient for solution of the equations herein to have them in nondimensional form, the following characteristic quantities were used to nondimensionalize the individual terms: for lengths, the shock-wave radius R_S' along the axis of symmetry; for velocity components, the free-stream velocity U_∞'; for density, the free-stream density ρ_∞'; for pressure, twice the free-stream dynamic pressure $\rho_\infty' U_\infty'^2$; for enthalpy, the square of the free-stream velocity $U_\infty'^2$; and for the radiation flux, the product of free-stream density and the cube of the free-stream velocity $\rho_\infty' U_\infty'^3$.

$c_1 = \frac{\partial p}{\partial h}$

$c_2 = \frac{\partial p}{\partial \rho}$

H total enthalpy

h static enthalpy

J number of equally spaced points along each ray at which radiative flux is calculated

K factor in governing equations, $K = 1 - Qy$

p	static pressure
Q	curvature of reference surface (shock wave)
$\bar{q}_R, q_R$	radiative heat-flux vector and its magnitude, respectively
R_b'	body radius of curvature
R_s'	radius of curvature of bow shock at $x = 0$, $R_s' \approx \left(R_b' + \delta_o'\right)$
r	radial distance from axis of symmetry of body (see fig. 1)
T'	temperature
u,v	velocity components in x- and y-directions, respectively
$\overline{V},U$	total velocity vector and its magnitude, respectively
x	coordinate measured along reference surface (shock wave)
x_i	a distance measured parallel to x-coordinate and downstream from it
y	coordinate measured normal to reference surface (shock wave)
z	axial coordinate from shock wave along axis of symmetry (see fig. 1)
δ	shock standoff distance
η	transformed y-coordinate, $\eta = 1 - \frac{y}{\delta}$
ρ	density
φ	azimuth angle (see eq. (A7))
ω	shock-wave angle (see fig. 1)
∇	del operator

Subscripts:

s	condition at shock
∞	free-stream conditions
o	conditions along stagnation streamline
SL	sea-level conditions

ANALYSIS

Governing Equations

The governing equations which describe an inviscid, nonconducting, radiating gas flow can be expressed in vector form as follows:

Continuity

$$\rho'\left(\nabla \cdot \overline{V}'\right) + \overline{V}' \cdot \nabla\rho' = 0 \tag{1}$$

Momentum

$$\left(\overline{V}' \cdot \nabla\right)\overline{V}' = -\frac{1}{\rho'}\nabla p' \tag{2}$$

Energy

$$\rho'\left(\overline{V}' \cdot \nabla H'\right) = -\nabla \cdot \bar{q}_R' \tag{3}$$

where

$$H' = h' + \frac{U'^2}{2} \tag{4}$$

In the inverse method of solution, the shape of the bow shock is given, and the shape of the body and the details of the flow in the shock layer are unknown. A curvilinear coordinate system is used in the present analysis, and thus the generalization of equations (1) to (4) is removed by relating these equations to a reference surface, the shock wave as depicted in figure 1. The coordinate x is defined on the surface as distance along the surface from the system symmetry axis. The coordinate y is the distance from the surface along a normal to the shock, defined as positive in the direction toward the body from the shock. The curvature of the reference surface is denoted by Q(x) defined as positive as shown.

The transposed equation (1) in terms of the shock-oriented coordinate system with dimensionless variables is written as follows:

Continuity

$$\frac{\partial(\rho u r)}{\partial x} + \frac{\partial(\rho v r K)}{\partial y} = 0 \tag{5}$$

where $K = 1 - Qy$.

Similarly, the momentum and energy equations can also be written as follows:

x-momentum

$$\frac{u}{K}\frac{\partial u}{\partial x} + v\frac{\partial u}{\partial y} - \frac{Q}{K}uv = -\frac{1}{\rho K}\frac{\partial p}{\partial x} \tag{6a}$$

y-momentum

$$\frac{u}{K}\frac{\partial v}{\partial x} + v\frac{\partial v}{\partial y} + \frac{Q}{K}u^2 = -\frac{1}{\rho}\frac{\partial p}{\partial y} \tag{6b}$$

Energy

$$\frac{u}{K}\frac{\partial H}{\partial x} + v\frac{\partial H}{\partial y} = -\frac{1}{\rho K r}\left[\frac{\partial(q_R r)}{\partial x} + \frac{\partial(q_R K r)}{\partial y}\right] \tag{7}$$

Note that replacing H with $h + \frac{u^2 + v^2}{2}$ in equation (7) gives

$$u\frac{\partial h}{\partial x} + u^2\frac{\partial u}{\partial x} + uv\frac{\partial v}{\partial x} + Kv\frac{\partial h}{\partial y} + Kuv\frac{\partial u}{\partial y} + Kv^2\frac{\partial v}{\partial y} = -\frac{1}{\rho r}\left[\frac{\partial(q_R r)}{\partial x} + \frac{\partial(q_R K r)}{\partial y}\right] \tag{8}$$

The shock layer is treated as a one-dimensional gas slab for purposes of radiative transport calculations. Thus, the term $\frac{\partial(q_R r)}{\partial x}$ in equation (8) is assumed to be negligible. A detailed development of the form of these equations as used in the numerical solution is given in the appendix.

The gas model used is equilibrium air. Thermodynamic properties are obtained by using the curve-fit technique described in reference 2.

Radiation Calculations

In order to find a numerical solution to equations (5), (6), and (8), the radiative-flux divergence term $\frac{\partial(q_R K r)}{\partial y}$ must be evaluated. Furthermore, one of the objectives of this program development is to use a reasonably detailed radiation model and avoid the use of gray gas or similar simplifications. The radiation model which was selected as being reasonably detailed but still compatible with the need for moderate computing times was developed for a radiation computer code called RATRAP (ref. 10). Local thermodynamic

and chemical equilibrium are assumed for the code, and a distribution of two thermodynamic variables must be known for the slab. (Pressure p' and enthalpy h' are used in the present analysis.) The radiation model for the RATRAP code is based on a nonuniform slab of high-temperature ($T' \geqq 10\ 000^{\circ}$ K) air plasma. RATRAP, as noted, does not use a gray-gas approximation but takes into account the frequency dependence of the radiation. Included in the model are self-absorption in the gas, atomic-line radiation, and the important continuum radiation processes. The radiation processes included are the continuum, line emission, and absorption for atomic N and O, the ions N^+ and O^+, electrons, and the O_2 Schumann-Runge continuum and N_2 Birge-Hopfield absorption band. This model was used without modification to calculate q_R wherever it appears in the present program.

Numerical Procedures

The numerical approach to this analysis is the inverse method, and the governing equations have been written in a form suitable for solution with this approach. The use of the inverse method for adiabatic flows has been well documented. (See, for example, refs. 1, 4, and 11.) A similar numerical approach is adopted for the present program, which is for nonadiabatic flows.

Briefly, the method consists of assuming a shock shape and a number of rays and their locations (fig. 1) and from the Rankine-Hugoniot relationships calculating the flow variables on each ray immediately behind the shock. The derivatives along the longitudinal coordinate (x-direction) can now be approximated by means of several mathematical schemes. For example, Van Dyke (ref. 12) used a series truncation method, whereas Marrone (ref. 11) used a seven-point polynomial fit to the calculated values. The latter approach is adopted for the present work (although the option exists of using a seven-point Lagrangian slope formula). Also, as an aid in delaying any tendency toward numerical instability, the flow variables are smoothed before taking derivatives in the x-direction. Smoothing was accomplished by using a least-square polynomial fit to each of the calculated flow variables. This method had the beneficial effect of allowing larger integration step sizes with the result that overall computing time was reduced. Substitution of the evaluated longitudinal derivatives into the governing partial differential equations leads to a set of ordinary differential equations with the normal coordinate (y-direction) as the independent variable. These ordinary differential equations represent a set of equations which can be solved numerically (for example, by using the fourth-order Runge-Kutta integration technique) in the sequence given in the appendix.

For an adiabatic flow-field solution by using the inverse method, the entire flow field is calculated for a given shock shape in a single pass. The presence of the radiative-flux term in the energy equation makes it necessary to resort to an iterative procedure in the

present program. The problem is begun with initial estimated distributions of pressure and static enthalpy along each ray, together with the length of the ray (i.e., the local standoff distance). This information is used as initial input to RATRAP, and initial values of the net radiative flux are calculated at J points along each ray. The local product Krq_R is formed at each point and derivatives in the y-direction are found by using a standard Lagrangian n-point differentiation formula. Since the tangent-slab approximation is being used, the resulting derivative is the flux divergence term required in equations (7) and (8). The solution proceeds until the "body point" is found for all except the last six rays. The resulting enthalpy profiles, pressure profiles, and standoff distances are then used as initial values, and the problem is repeated until a predetermined convergence test is satisfied, at which time the solution is considered to be complete. The convergence test is based on the static enthalpy at selected discrete points in the shock layer. Static enthalpy was selected for the convergence tests because it is one of the most sensitive parameters in the radiating gas flow calculations. The allowable error in h used for the enthalpy convergence test was ±0.006. Some calculations were made with the test value set at ±0.001, but the number of iterations greatly increased without any significant changes in the final results. No case has been found in which the iteration technique failed to converge to a solution.

Since testing for convergence at every point in the flow field is not feasible, the test points were selected to be uniformly distributed throughout the flow field but included critical points where the enthalpy gradients are greatest. These test points do not, however, include the last calculated y-station (body point) on any ray. It was originally planned to include these points, but the numerical problems associated with the mass balance, which are discussed subsequently, precluded their use.

An effort was made to establish the influence of the initial estimated profiles on the rate of convergence. The solution was found to converge for almost any reasonable estimate, but starting from the adiabatic profiles added one extra iteration. From experience it was found that the following procedure for establishing initial values gave consistently good results. For the pressure profile, the pressure is assumed to be invariant along each ray at a value obtained for the local oblique shock in a perfect gas. This value can be obtained from reference 13. For the standoff distance, the dimensionless standoff distance is assumed to vary with x according to the expression

$$\delta = 0.0392 + 0.022x \tag{9}$$

Finally, for the enthalpy profile, the enthalpy is assumed to vary with δ so that

$$h = \left(\frac{2\delta - y}{2\delta}\right) H_\infty \tag{10}$$

These equations, which were derived from adiabatic results and a linear approximation to the nonadiabatic results of reference 5, have been used extensively for both strongly and weakly radiating flows, and no case has been found in which convergence was not rapid.

Three numerical procedure problems, which require some discussion, were encountered. These problems are enthalpy profile damping, ray dropping, and satisfying the mass balance.

Enthalpy profile damping.- Initial calculations with the program showed that the solution did not converge in any reasonable number of iterations. The problem stemmed from the use of the updated enthalpy profile in each iteration without modification, and in some cases this use was sufficient to cause oscillation. This problem was handled by incorporating the following expression for updating enthalpies:

$$h = h_g - G(h_g - h_p)$$

where

G damping coefficient

h_g enthalpy currently generated

h_p enthalpy previously generated

Several values of G were tried and it was found that a value of $G = 0.35$ gave good results. This value has been incorporated into the program. The damping equation is not used until the start of the second iteration. Generally though, only two iterations are required after damping is introduced.

Ray dropping.- As previously noted, the seven-point polynomial-fit technique (ref. 11) was used when taking derivatives in the x-direction. This technique was selected because of the excellent results obtained from its application to adiabatic flow, which does not require an iterative solution. The technique, as noted in reference 11, calculates derivatives until there are six rays which have not "reached the body" (i.e., satisfied the arbitrary mass-conservation criterion). For an adiabatic flow, these last six rays are then discarded and the solution is considered to be complete.

If carried over intact to the nonadiabatic flow, this numerical scheme would require that six rays be discarded at the end of each iteration. This procedure would seriously limit the number of iterations (maximum of three for the present program) and the x-distance covered by any solution. The calculated values from these rays are used only to provide updated p', h', and δ' solutions for RATRAP. To circumvent this difficulty, the initial total number of rays was retained, a procedure equivalent to assuming that the

last calculated values on each of these rays represented results at the body station. In the final solution the results from the last six rays are ignored since the calculations always show that they have not reached the body. The calculations do, however, show that the profiles along these rays are not so distorted that their use will influence the answers for the rays which do reach the body.

Satisfying the mass balance.- Since the inverse method starts with a given shock shape, one of the problems which is encountered in its use is establishing when the body is reached. The normal approach is to calculate the mass flow crossing the shock wave between the stagnation streamline and the ray in question and balance this against the mass flow crossing the ray as the flow is integrated in the y-direction. Reference 11 shows that computing time becomes excessive as the mass-balance ratio becomes very close to 1.0, and the body shape associated with a ratio of 0.98 is indistinguishable from the body associated with a ratio of 0.995. Thus, the mass-balance test for a body point was initially set at 0.98 for the present program. It was soon discovered that because of the nonadiabatic nature of the problem, oscillations appeared in the enthalpy distribution around the body. Furthermore, in some cases these oscillations tended to diverge with succeeding iterations so that it was not possible to obtain a solution. These oscillations were not present in the enthalpy distributions for a mass-balance ratio of 0.96. Therefore, the mass-balance ratio requirement was lowered from 0.98 to 0.96 with the result that the oscillations did not appear and solutions were found for all cases.

The influence of this change in mass-balance ratio requirement was investigated in the following manner. A series of solutions was calculated for several flight conditions with mass-balance ratio requirement values of 0.95, 0.96, 0.97, and where possible 0.98. The stagnation-streamline (ray 1) results of these solutions were plotted as standoff distance as a function of mass-balance ratio, and the resulting curves were linearly extrapolated to mass-balance ratios of 1.0. It was found that the standoff distance with a 0.96 mass-balance ratio was 90.4 ($\pm$2.5) percent of the value for a mass-balance ratio of 1.0. This extrapolation technique has been applied to all values of δ presented in this report except those for adiabatic flows for which the results with a 0.98 mass-balance ratio were considered adequate. Comparisons of enthalpy profiles from the present method with those from other methods, which will be shown subsequently, indicate that the present method is suitable for finding δ.

In some cases, the solution did not oscillate but it did contain irregularities in the enthalpy distribution around the body at the last calculated y-station. These irregularities were traced to the seven-point numerical scheme used for taking derivatives in the x-direction. This scheme slides along the rays considering the first seven rays for which the body point has not been reached. When a ray reaches the body, it is removed from the calculation, and another ray is picked up to take its place. When the solution proceeds in

an orderly fashion so that rays drop out of the calculation one at a time, the numerical scheme produces a very regular enthalpy profile. However, in some cases the mass-balance ratio requirement is met on several rays during the same Runge-Kutta integration step. When this occurs all these rays are removed at once, and the numerical scheme is forced to jump several rays; derivatives, which after one integration step are calculated by central difference formulas, are calculated by end-point formulas after the next integration step. It would be possible to overcome this difficulty by reducing the integration step size, but this has not been done because the error introduced was not sufficient to justify the additional computing time. For the static enthalpy profile, however, the error may be sufficiently large to preclude the use of the last calculated y-station on each ray when calculating values for the convergence test. Consequently, these points have not been used when testing for convergence.

Program Restrictions

The program, as written, has several restrictions which must be noted. First, the assumed shock must be analytic in shape. Experience has shown that if the shock is not analytic, the program will not function properly. This restriction need not impair the usefulness of the program since many bodies can be found for which the shock approximately meets this requirement. All the results given herein were calculated for the case of a catenary shock which produces a nearly spherical body. Second, the solution is confined to the subsonic part of the gas cap. Extension to the supersonic region would require conversion to a method-of-characteristics solution such as used in reference 4.

Finally, as written, the program is restricted in the number of rays and radiative flux points J which can be used. The number of rays must be greater than or equal to 8 and less than or equal to 24. The value of J must be 5, 7, 9, or 11. These limitations are not inherent in the inverse method but are the result of programing and machine storage requirements.

RESULTS AND DISCUSSION

The inverse flow-field program already described has been used with a catenary shock shape to calculate flow fields for a number of cases with a wide range of velocities, densities, and body sizes (table 1). In all cases the catenary shock shape produced a nearly spherical body. These cases, in general, cover flight conditions for which the postshock equilibrium temperature is between 10 000° K and 15 000° K and hence is within the range of applicability of both RATRAP and the air correlations of reference 2. The effects of varying the number of rays in the flow field and the number of points along each ray at which the radiation heat fluxes were obtained from RATRAP have also been studied to investigate the influence of the finite-difference mesh size on the calculated results and

the influence of the number of RATRAP calculation points on the accuracy of the flux divergence calculations. These cases are listed in table 2. In tables 1 and 2 the body radius R'_b was determined by subtracting the final calculated standoff distance δ' from the input stagnation-streamline shock radius R'_s. Since the body radius is determined in this manner, it is not surprising that slight differences appear between the calculated R'_b and the reference values in tables 1 and 2.

Nonradiating Solutions

In order to verify that the program was functioning properly, a nonradiating test case was conducted for comparison with the results of reference 2, in which the integral method was compared with the inverse method of Lomax and Inouye (ref. 4). The comparisons are shown in figure 2. As can be seen, the results from the three programs are generally in agreement. However, the results from the two inverse programs are in closer agreement, except for the density profiles close to the stagnation streamline. The differences that existed there, approximately 3 to 4 percent, are apparently the result of the different thermodynamic models used. The present program and reference 2 used the same air properties model whereas reference 4 used a different model. (Ref. 2 presents data which show that the air model of ref. 4 may be slightly more precise than the model used for the present work.)

Radiating Solutions

The influence of the nonadiabatic effect of radiation cooling, as well as the effects of body size and velocity, has been studied. The results are shown in figures 3 to 7. Figure 3 compares the nonadiabatic and adiabatic results calculated for a large body $\left(R'_b = 343.80 \text{ cm}\right)$ at a high velocity $\left(U'_\infty = 14.55 \text{ km/sec}\right)$. Various flow properties are plotted as a function of dimensionless shock-layer thickness for two rays, $x = 0.009$ and $x = 0.254$. The ray at $x = 0.009$ is the first ray in the mesh and will be referred to as ray 1. Since this ray is very close to the stagnation streamline, the calculated values for this ray have been assumed to be stagnation-streamline values. The ray at $x = 0.254$ is typical of a ray far from ray 1. Note that the pressure profile (fig. 3(c)) is not materially changed by the nonadiabatic effects, but all the other flow properties experience significant changes. As figure 3(e) shows, the standoff distance is decreased by approximately 25 percent, but the resulting body remains nearly spherical.

Figures 4 and 5 show the influence of body size on the ray 1 (stagnation streamline) enthalpy profiles for two different flight conditions. It can be seen that the nonadiabatic effects decrease with decreasing body size. The influence of the free-stream velocity is shown in figure 6, where the influence of body size and density have been eliminated. The decrease in nonadiabatic effects with decreasing velocity is evident.

Figure 7 shows a plot of enthalpy at the last calculated y-station for ray 1 as a function of free-stream velocity for two extreme values of free-stream density and for a large body. Note that the enthalpy extrapolates to the adiabatic value (0.5) for both densities at $U'_\infty \cong 9$ km/sec. From the results shown in figures 3 to 7, it is concluded that an adiabatic solution is always justified for flight velocities of 9 km/sec or less and for bodies with R'_b of about 3 cm or less. For flight velocities of 10 km/sec or higher and bodies with R'_b larger than about 3 cm, the nonadiabatic effects become significant, and an adiabatic solution could result in serious error.

Radiating Solution Comparisons

As previously indicated, one of the objectives of the present program development was to provide an independent check on other flow-field programs, particularly the method of integral relations or direct method (ref. 5). Comparisons have been made with the direct method (ref. 5) which uses the same thermodynamic and radiation models and with the time-dependent method from reference 6. Results from these comparisons are shown in figures 8 to 11.

Figure 8 shows a comparison between the present results and those from reference 5. The figure shows the flux distributions around the body for one adiabatic case $R'_b = 342.7$ cm (ref. 5) and two nonadiabatic cases. The adiabatic case shows excellent agreement in the stagnation region ($0 \leqq x \leqq 0.15$), but shows a continually increasing divergence for $x \geqq 0.15$. At $x = 0.465$ the difference is approximately 15 percent, based on the inverse solution. A comparison of the details of the two sets of results shows that in the stagnation region the standoff distance, pressure profile, and static enthalpy profile are identical, but at the larger values of x, differences appear in the standoff distance, shock curvature, pressure profile, and enthalpy profile. The flux distributions shown represent the cumulative effect of all these variations so that the spread shown is indicative of the comparative differences of the two methods for an adiabatic case.

The comparative nonadiabatic flux distributions for two body sizes are also shown in figure 8. For $0 \leqq x \leqq 0.254$, the results generally agree within 5 percent. For $x > 0.254$, the inverse-method results show the influence of modifying the ray-dropping procedure. The results from the last six rays (broken symbols in fig. 8) are known to be in error since the mass flow is never balanced (but never more than 10 percent out of balance) on these rays and the body point and flux profiles are never completely determined. This kind of check shows that for nonadiabatic flow fields, either of the programs shown will produce radiative-flux values of comparable accuracy.

Stagnation-streamline (ray 1) profiles of total enthalpy, density, temperature, and pressure for the nonadiabatic cases of figure 8 are shown in figure 9. The general level of agreement is good for both cases but definitely much better for the smaller body

$\left(R_b' = 34.27 \text{ cm}\right)$. This effect is due to the previously noted fact that as body size decreases, the stagnation-streamline profiles approach the adiabatic values, which are in good agreement for the results from both programs. A comparison of the curves for the larger body $\left(R_b' = 342.7 \text{ cm}\right)$ shows that as expected, the direct method does not give as much detail as the inverse method. Figure 9 also emphasizes that the inverse nonadiabatic calculations do not reach the body station. The last calculated point is at $\eta \cong 0.095$ which is consistent with a mass-balance ratio of 0.96.

In figure 10 are shown results taken from reference 6 for nondimensional enthalpy profiles along the stagnation streamline and those computed from the present program. Reference 6 uses a second-order time-asymptotic technique for computing a nongray, nonadiabatic absorbing flow field around a blunt body. The radiation model used in reference 6 was the three-step model approximation. The results taken from reference 6 for comparison were based on a body nose radius of 2 meters and free-stream velocities of 10 km/sec and 14 km/sec at a density ratio of 10^{-3} (equivalent altitude of 48.5 km). These results compared favorably with those computed from the present program for a velocity of 10 km/sec. (For this velocity, the radiation effects appear to be small but still nonadiabatic.) Also, for 14 km/sec where radiation effects are large, the two programs give results which differ at most by 10 percent. Some insight into this difference may be gained by examining the results for the low velocity. Here the radiation effects were small, and with the results in agreement, the conclusion can be drawn for nearly adiabatic flows that these methods for computing flow fields give comparable stagnation-streamline solutions. Hence, for the high velocity, the two remaining factors which can contribute to the 10-percent difference in results are the influence of strong radiation in the flow-field solution methods and the radiation models used. No attempt was made to isolate which of these two factors was dominant.

Figure 11 shows results from three different flow-field computational techniques, the present inverse method, the direct method, and the time-asymptotic method. The effect of radiation on the enthalpy profile along the stagnation streamline is shown here for two body sizes, $R_b' = 34.27$ cm and $R_b' = 342.7$ cm. The body sizes and flow conditions were the original ones used in reference 5. The direct method and inverse method used the same thermodynamic and radiation models while the time-asymptotic technique used the three-step radiation model and thermodynamic model described in reference 6. The results from the direct method and inverse method are in agreement for the small body $\left(R_b' = 34.27 \text{ cm}\right)$ whereas for the large body $\left(R_b' = 342.7 \text{ cm}\right)$, the time-asymptotic scheme and inverse-method results agreed more favorably and displayed characteristically similar enthalpy profiles.

A final comparison with published results is shown in figure 12, where the flux and temperature profiles calculated by the present program are compared with the results

from reference 14. Reference 14 considers a stagnation streamline only, integrates from the body to the shock, uses its own radiation and thermodynamic models, retains viscous effects in the momentum equation, and ignores the influence of curvature on the pressure gradient. A brief study showed that the dominant factor in the differences in figure 12 is the continuum radiation model used in reference 14. This model uses a hydrogenic approximation which gives questionable absorption coefficients in certain spectral regions and distorts the flux profiles across the shock layer. The difference shown is similar to that shown in reference 15, which uses the inviscid flow-field calculations of reference 5. In view of the agreement already shown (figs. 8, 9, and 11) between the present method and reference 5, the differences shown in figure 12 are not surprising.

Program Characteristics

The results shown were obtained with the present program operating with what is considered a nominal mesh configuration, 14 rays spaced $\Delta x = 0.0351$ apart and 9 radiative flux calculations performed on each ray. The final part of the program development was devoted to an investigation of the rate of convergence and the influence of changing the number of rays, the ray spacing, and the number of radiative flux points on the final results. In all cases, the first ray was located at $x = 0.009$ from the axis of symmetry. The cases considered are given in table 2.

The rate of convergence of the solution for a mesh with 14 rays and the radiative flux calculated at 9 points along each ray is shown in figure 13. Here the stagnation enthalpy profiles for the initial inputs through the fourth and final solution are shown. As illustrated by this plot, the solutions converge rapidly; convergence and the final solution are realized after the enthalpy accuracy criterion (± 0.006) is satisfied. Note that for this case in the area of the body station the enthalpy convergence test is not satisfied between the third and fourth solutions because of the numerical procedural problem of forming the x-derivatives. The case shown took 8 minutes on the Control Data Series 6000 computer system. Computing times, however, are strongly dependent on the body size, free-stream velocity and density, the number of rays, and the number of points J along each ray at which the radiative heat flux is obtained from RATRAP.

The effect of varying the number of rays from 10, $\Delta x = 0.0507$ to 20, $\Delta x = 0.0240$, for a fixed number of radiation heat-flux points along each ray is shown in figure 14 for a body radius of 34.44 cm. The effect on the stagnation enthalpy profile is negligible; any differences which may exist are within the order of accuracy for h (± 0.006). These results are typical for even those profiles away from the stagnation streamline. Also, varying J from 5 to 11 along each ray and keeping the number of rays fixed at 14 for the same conditions above indicate negligible effects on the stagnation enthalpy profile, as shown in figure 15. However, the same conclusions cannot be drawn when the body

size is increased by approximately an order of magnitude. Here the effects are sizable in going from 10 rays and $J = 5$ to 14 rays and $J = 9$, as shown in figure 16. However, the differences become negligible when going from 14 rays and $J = 9$ to 20 rays and $J = 11$. On the basis of these results, it can be concluded that for general operation of the program, the nominal mesh configuration will produce good results over the entire range of applicability of the program. For smaller bodies or lower speeds, a much coarser mesh can be used to reduce computing time with no loss in accuracy. For the largest bodies and highest speeds considered, the gain in accuracy obtained by going to 20 rays does not warrant the increased computer time.

CONCLUDING REMARKS

An inverse flow-field program capable of making calculations with an equilibrium air gas model and a realistic radiation model has been developed. The program is capable of calculating the inviscid flow field on a blunt body over a very large range of conditions. The primary restrictions are that the assumed shock be analytic in shape and that the postshock temperature be between 10 000° K and 15 000° K.

Results calculated by using the present inverse-method program have been compared with results obtained from a direct-method program and a time-asymptotic-method program. In general, the comparisons indicate substantial agreement among all three programs. However, the inverse method does retain more of the details of the flow than the direct method and therefore may be more valuable in certain instances. The degree of comparison between the inverse method, the time-asymptotic method of Callis (NASA TR R-299), and the stagnation-streamline solution of Rigdon, Dirling, and Thomas (NASA CR-1462) is clouded by variations in the thermodynamic and radiation models used. In general, the comparisons can be considered good.

The inverse method can be operated with 8 to 24 rays and with 5, 7, 9, or 11 radiative flux calculations along each ray. A brief study has shown that a nominal set of 14 rays and 9 radiative-flux calculations will produce accurate results over the entire range of applicability of the program. The use of more rays and/or more flux points results in no substantial increase in accuracy. The use of fewer rays and/or fewer flux points will save on computer time, but for larger bodies or higher flow velocities, a marked decrease in accuracy is noted.

Langley Research Center,
National Aeronautics and Space Administration,
Hampton, Va., June 22, 1970.

APPENDIX

DEVELOPMENT OF THE NUMERICALLY INTEGRATED GOVERNING EQUATIONS

This appendix gives a detailed derivation of the governing differential equations (eqs. (5), (6), and (8)) and the procedure required to reduce them to a form suitable for sequential solution on a high-speed digital computer. The governing flow equations for an inviscid, nonconducting, radiating gas are given in vector form as

Continuity

$$\rho'\left(\nabla \cdot \overline{V}'\right) + \overline{V}' \cdot \nabla\rho' = 0 \tag{A1}$$

Momentum

$$\left(\overline{V}' \cdot \nabla\right)\overline{V}' = -\frac{1}{\rho'} \nabla p' \tag{A2}$$

Energy

$$\rho'\left(\overline{V}' \cdot \nabla H'\right) = -\nabla \cdot \bar{q}_R' \tag{A3}$$

where

$$H' = h' + \frac{U'^2}{2} \tag{A4}$$

Primes in equations (A1) to (A4) refer to dimensional quantities.

An elemental distance in the x-direction in terms of an elemental distance along the shock is (fig. 1)

$$dx_i' = \left(1 - Q'y'\right)dx' \tag{A5}$$

and letting $K' = 1 - Q'y'$ reduces the elemental arc dx_i' to

$$dx_i' = K'\,dx' \tag{A6}$$

An element of arc ds' in three-dimensional coordinates, is

$$ds'^2 = K'^2 dx'^2 + dy'^2 + r'^2 d\varphi^2 \tag{A7}$$

where φ is the azimuth angle.

Thus, with this metric equation the relation between a general orthogonal coordinate system and a specific shock-oriented one is established. Note that the coordinate system is curvilinear and orthogonal.

Then, the continuity equation (A1) in terms of the shock-oriented coordinate system with dimensionless variables and for an axisymmetrical condition can be written as follows:

Continuity

$$\frac{\partial(\rho u r)}{\partial x} + \frac{\partial(\rho v r K)}{\partial y} = 0 \tag{A8}$$

Similarly, the momentum and energy equations can also be written as follows:

x-momentum

$$\frac{u}{K}\frac{\partial u}{\partial x} + v\frac{\partial u}{\partial y} - \frac{Q}{K}uv = -\frac{1}{\rho K}\frac{\partial p}{\partial x} \tag{A9}$$

y-momentum

$$\frac{u}{K}\frac{\partial v}{\partial x} + v\frac{\partial v}{\partial y} + \frac{Q}{K}u^2 = -\frac{1}{\rho}\frac{\partial p}{\partial y} \tag{A10}$$

Energy

$$\frac{u}{K}\frac{\partial H}{\partial x} + v\frac{\partial H}{\partial y} = -\frac{1}{\rho K r}\left[\frac{\partial(q_R r)}{\partial x} + \frac{\partial(q_R K r)}{\partial y}\right] \tag{A11}$$

Note that replacing H with $h + \frac{u^2 + v^2}{2}$ in equation (A11) gives

$$u\frac{\partial h}{\partial x} + u^2\frac{\partial u}{\partial x} + uv\frac{\partial v}{\partial x} + Kv\frac{\partial h}{\partial y} + Kuv\frac{\partial u}{\partial y} + Kv^2\frac{\partial v}{\partial y} = -\frac{1}{\rho r}\left[\frac{\partial(q_R r)}{\partial x} + \frac{\partial(q_R K r)}{\partial y}\right] \tag{A12}$$

The assumption of an infinite slab is used; thus, the term $\frac{\partial(q_R r)}{\partial x}$ in equation (A12) is assumed to be negligible. The energy equation is written

$$u\frac{\partial h}{\partial x} + u^2\frac{\partial u}{\partial x} + uv\frac{\partial v}{\partial x} + Kv\frac{\partial h}{\partial y} + Kuv\frac{\partial u}{\partial y} + Kv^2\frac{\partial v}{\partial y} + \frac{1}{\rho r}\frac{\partial(q_R K r)}{\partial y} = 0 \tag{A13}$$

The equation of state is also utilized here

$$p = p(h, \rho) \tag{A14}$$

These governing equations must now be manipulated so that the partial differential equations of the flow variables u, ρ, v, p, and h are obtained. Furthermore, the resulting equations should be written in a form suitable for sequential solution by using standard numerical techniques as mentioned previously.

The term $\partial u/\partial y$ is obtained directly from the x-momentum equation (eq. (A9)).

$$\frac{\partial u}{\partial y} = -\frac{1}{Kv}\left(\frac{1}{\rho}\frac{\partial p}{\partial x} + u\frac{\partial u}{\partial x} - Quv\right) \tag{A15}$$

Note that since the inverse method is being used, all derivatives with respect to x can be assumed known for the purpose of this derivation.

APPENDIX

Next the y-momentum, energy, and state equations (eqs. (A10), (A13), and (A14)) are combined to obtain an expression for $\partial v/\partial y$ in terms of $\partial \rho/\partial y$. The steps involved are as follows:

From equation (A13), solve for $\partial v/\partial y$

$$\frac{\partial v}{\partial y} = -\frac{1}{Kv^2}\left[u^2 \frac{\partial u}{\partial x} + uv \frac{\partial v}{\partial x} + u \frac{\partial h}{\partial x} + Kv \frac{\partial h}{\partial y} + Kuv \frac{\partial u}{\partial y} + \frac{1}{\rho r} \frac{\partial (q_R Kr)}{\partial y}\right] \tag{A16}$$

Differentiate equation (A14) with respect to y and solve for $\partial h/\partial y$

$$\frac{\partial p}{\partial y} = \frac{\partial p}{\partial h} \frac{\partial h}{\partial y} + \frac{\partial p}{\partial \rho} \frac{\partial \rho}{\partial y} \tag{A17}$$

$$\frac{\partial h}{\partial y} = \frac{1}{c_1}\left(\frac{\partial p}{\partial y} - c_2 \frac{\partial \rho}{\partial y}\right) \tag{A18}$$

where $c_1 = \partial p/\partial h$ and $c_2 = \partial p/\partial \rho$. The terms c_1 and c_2 are available from the correlation of equilibrium air properties to 15 000° K described in reference 10. Substituting the expression for $\partial h/\partial y$ (eq. (A18)) into equation (A16) gives

$$\frac{\partial v}{\partial y} = -\frac{1}{Kv^2}\left[u^2 \frac{\partial u}{\partial x} + uv \frac{\partial v}{\partial x} + u \frac{\partial h}{\partial x} + \frac{Kv}{c_1}\left(\frac{\partial p}{\partial y} - c_2 \frac{\partial \rho}{\partial y}\right) + Kuv \frac{\partial u}{\partial y} + \frac{1}{\rho r} \frac{\partial (q_R Kr)}{\partial y}\right] \tag{A19}$$

Replacing $\partial p/\partial y$ in equation (A19) by its equivalence from the y-momentum equation (A10) and collecting all terms in $\partial v/\partial y$ gives

$$\frac{\partial v}{\partial y}\left(1 - \frac{\rho}{c_1}\right) = -\frac{1}{Kv^2}\left[u^2 \frac{\partial u}{\partial x} + uv \frac{\partial v}{\partial x} + u \frac{\partial h}{\partial x} - \frac{\rho uv}{c_1} \frac{\partial v}{\partial x} - \frac{Q\rho u^2 v}{c_1} - \frac{Kvc_2}{c_1} \frac{\partial \rho}{\partial y} + Kuv \frac{\partial u}{\partial y} + \frac{1}{\rho r} \frac{\partial (q_R Kr)}{\partial y}\right] \tag{A20}$$

Equation (A20) is the desired equation for $\partial v/\partial y$ in terms of $\partial \rho/\partial y$. Equations (A20) and (A8) now form a set of two equations in two unknowns which can be solved as follows:

From equation (A8)

$$\frac{\partial \rho}{\partial y} = -\frac{\rho}{Kv}\left(\frac{u}{\rho} \frac{\partial \rho}{\partial x} + \frac{\partial u}{\partial x} + \frac{u}{r} \frac{\partial r}{\partial x} + K \frac{\partial v}{\partial y} + \frac{Kv}{r} \frac{\partial r}{\partial y} - Qv\right) \tag{A21}$$

APPENDIX

The expression in equation (A20) for $\partial v/\partial y$ is substituted into equation (A21) to give

$$\frac{\partial \rho}{\partial y} = -\frac{v\left(1 - \frac{\rho}{c_1}\right)}{K\left(\frac{v^2}{\rho} + \frac{c_2 - v^2}{c_1}\right)}\left(\frac{u}{\rho}\frac{\partial \rho}{\partial x} + \frac{\partial u}{\partial x} + \frac{u}{r}\frac{\partial r}{\partial x} + \frac{Kv}{r}\frac{\partial r}{\partial y} - Qv\right) + \frac{1}{Kv\left(\frac{v^2}{\rho} + \frac{c_2 - v^2}{c_1}\right)}$$

$$\times\left[uv\left(1 - \frac{\rho}{c_1}\right)\frac{\partial v}{\partial x} + u\frac{\partial h}{\partial x} - \frac{Q\rho u^2 v}{c_1} + Kuv\frac{\partial u}{\partial y} + \frac{1}{\rho r}\frac{\partial\left(q_R Kr\right)}{\partial y} + u^2\frac{\partial u}{\partial x}\right] \qquad \text{(A22)}$$

Thus, once $\partial\rho/\partial y$ has been evaluated with equation (A22), then $\partial v/\partial y$ can be evaluated with equation (A20). Now all information is available to evaluate $\partial p/\partial y$ from the y-momentum equation (eq. (A10)). Finally, $\partial h/\partial y$ is evaluated from equation (A18).

In summary, the final set of partial differential equations (eqs. (A15), (A22), (A20), (A10), and (A18)) used in the program, listed in the order in which they are evaluated, is

$$\frac{\partial u}{\partial y} = -\frac{1}{Kv}\left(\frac{1}{\rho}\frac{\partial p}{\partial x} + u\frac{\partial u}{\partial x} - Quv\right)$$

$$\frac{\partial \rho}{\partial y} = -\frac{v\left(1 - \frac{\rho}{c_1}\right)}{K\left(\frac{v^2}{\rho} + \frac{c_2 - v^2}{c_1}\right)}\left(\frac{u}{\rho}\frac{\partial \rho}{\partial x} + \frac{\partial u}{\partial x} + \frac{u}{r}\frac{\partial r}{\partial x} + \frac{Kv}{r}\frac{\partial r}{\partial y} - Qv\right) + \frac{1}{Kv\left(\frac{v^2}{\rho} + \frac{c_2 - v^2}{c_1}\right)}$$

$$\times\left[uv\left(1 - \frac{\rho}{c_1}\right)\frac{\partial v}{\partial x} + u^2\frac{\partial u}{\partial x} + u\frac{\partial h}{\partial x} - \frac{Q\rho u^2 v}{c_1} + Kuv\frac{\partial u}{\partial y} + \frac{1}{\rho r}\frac{\partial\left(q_R Kr\right)}{\partial y}\right]$$

$$\frac{\partial v}{\partial y} = -\frac{1}{Kv^2\left(1 - \frac{\rho}{c_1}\right)}\left[u^2\frac{\partial u}{\partial x} + uv\frac{\partial v}{\partial x} + u\frac{\partial h}{\partial x} - \frac{\rho uv}{c_1}\frac{\partial v}{\partial x} - \frac{Q\rho u^2 v}{c_1} - \frac{Kvc_2}{c_1}\frac{\partial \rho}{\partial y}\right.$$

$$\left. + Kuv\frac{\partial u}{\partial y} + \frac{1}{\rho r}\frac{\partial\left(q_R Kr\right)}{\partial y}\right]$$

$$\frac{\partial p}{\partial y} = -\rho\left(\frac{u}{K}\frac{\partial v}{\partial x} + v\frac{\partial v}{\partial y} + \frac{Q}{K}u^2\right)$$

$$\frac{\partial h}{\partial y} = \frac{1}{c_1}\left(\frac{\partial p}{\partial y} - c_2\frac{\partial \rho}{\partial y}\right)$$

REFERENCES

1. Hayes, Wallace D.; and Probstein, Ronald F.: Hypersonic Flow Theory. Vol. I – Inviscid Flows. Second ed., Academic Press, 1966.

2. Garrett, L. Bernard; Suttles, John T.; and Perkins, John N. (With appendix C by G. Louis Smith and L. Bernard Garrett): A Modified Method of Integral Relations Approach to the Blunt-Body Equilibrium Air Flow Field, Including Comparisons With Inverse Solutions. NASA TN D-5434, 1969.

3. Moretti, Gino; and Abbett, Michael: A Time-Dependent Computational Method for Blunt Body Flows. AIAA J., vol. 4, no. 12, Dec. 1966, pp. 2136-2141.

4. Lomax, Harvard; and Inouye, Mamoru: Numerical Analysis of Flow Properties About Blunt Bodies Moving at Supersonic Speeds in an Equilibrium Gas. NASA TR R-204, 1964.

5. Suttles, John T.: A Method of Integral Relations Solution for Radiating, Nonadiabatic, Inviscid Flow Over a Blunt Body. NASA TN D-5480, 1969.

6. Callis, Linwood B.: Solutions of Blunt-Body Stagnation-Region Flows With Nongray Emission and Absorption of Radiation by a Time-Asymptotic Technique. NASA TR R-299, 1969.

7. Cheng, Ping; and Vincenti, Walter G.: Inviscid Radiating Flow Over a Blunt Body. J. Fluid Mech., vol. 27, pt. 4, Mar. 1967, pp. 625-646.

8. Olstad, W. B.: Nongray Radiating Flow About Smooth Symmetric Bodies With Large Blowing. AIAA Pap. No. 69-637, June 1969.

9. Maslen, S. H.: Inviscid Hypersonic Flow Past Smooth Symmetric Bodies. AIAA J., vol. 2, no. 6, June 1964, pp. 1055-1061.

10. Wilson, K. H.: RATRAP – A Radiation Transport Code. 6-77-67-12, Lockheed Missiles & Space Co., Mar. 14, 1967.

11. Marrone, Paul V.: Inviscid, Nonequilibrium Flow Behind Bow and Normal Shock Waves, Part I. General Analysis and Numerical Examples. Rep. No. QM-1626-A-12(I) (Contract No. DA-30-069-ORD-3443), Cornell Aeronaut. Lab., Inc., May 1963.

12. Van Dyke, Milton: Hypersonic Flow Behind a Paraboloidal Shock Wave. J. Mecan., vol. 4, no. 4, Dec. 1965, pp. 477-493.

13. Ames Research Staff: Equations, Tables, and Charts for Compressible Flow. NACA Rep. 1135, 1953. (Supersedes NACA TN 1428.)

14. Rigdon, W. S.; Dirling, R. B., Jr.; and Thomas, M.: Stagnation Point Heat Transfer During Hypervelocity Atmospheric Entry. NASA CR-1462, 1970.

15. Smith, G. Louis; Suttles, John T.; Sullivan, Edward M.; and Graves, Randolph A., Jr.: Viscous Radiating Flow Field on an Ablating Blunt Body. AIAA Pap. No. 70-218, Jan. 1970.

TABLE 1.- RANGE OF VELOCITIES, DENSITIES, AND BODY SIZES STUDIED INCLUDING COMPARATIVE CONDITIONS

ρ_∞/ρ_{SL}	U_∞, km/sec	R_s, cm	R'_b, cm		Remarks
			Inverse method	Reference	
2.2064×10^{-4}	15.25	3.105 31.9 314.85	2.971 30.7 304.4	3.05 30.5 305	Velocity and body size (by two orders of magnitude) varied at altitude of 61 km
2.2064×10^{-4}	12.81	314.85	302.9	305	
2.2064×10^{-4}	10.37	314.85 3.105	300.8 2.961	305 3.05	
1.392×10^{-2}	11.59	3.105 31.9 314.85	2.945 30.30 300.3	3.05 30.5 305	Velocity and body size (by two orders of magnitude) varied at altitude of 30.5 km
1.392×10^{-2}	9.455	31.9 314.85	30.4 298.6	30.5 305	
1.84×10^{-4}	14.55	356.16 35.84	343.8 34.44	342.7 34.27	Conditions of reference 5
1.0×10^{-3}	14 10	208 209.5	199.50 199.50	200 200	Conditions of reference 6

TABLE 2.- INFORMATION USED TO ESTABLISH FLOW-FIELD MESH SIZES

ρ_∞/ρ_{SL}	U'_∞, km/sec	R'_b, cm	Number of rays	Spacing of rays, Δx	Number of radiative flux points along each ray, J	Remarks
1.84×10^{-4}	14.55	34.44	20	2.401×10^{-2}	5	Number of rays varied, total x-distance fixed at 0.464, and J = 5
			10	5.07×10^{-2}		
			14	3.509×10^{-2}		
1.84×10^{-4}	14.55	34.44	14	3.509×10^{-2}	9	Only J varied
					11	
1.84×10^{-4}	14.55	34.44	10	5.07×10^{-2}	11	Effect of minimum number of rays used and maximum J
1.84×10^{-4}	14.55	34.44	20	3.509×10^{-2}	5	Increased x to 0.675 for minimum J
2.2064×10^{-4}	15.25	304.4	10	5.07×10^{-2}	5	Effect of changing number of rays and J on large body and high velocity and altitude
			14	3.509×10^{-2}	9	
			20	2.401×10^{-2}	11	
2.2064×10^{-4}	12.81	302.9	10	5.07×10^{-2}	5	
			14	3.509×10^{-2}	9	

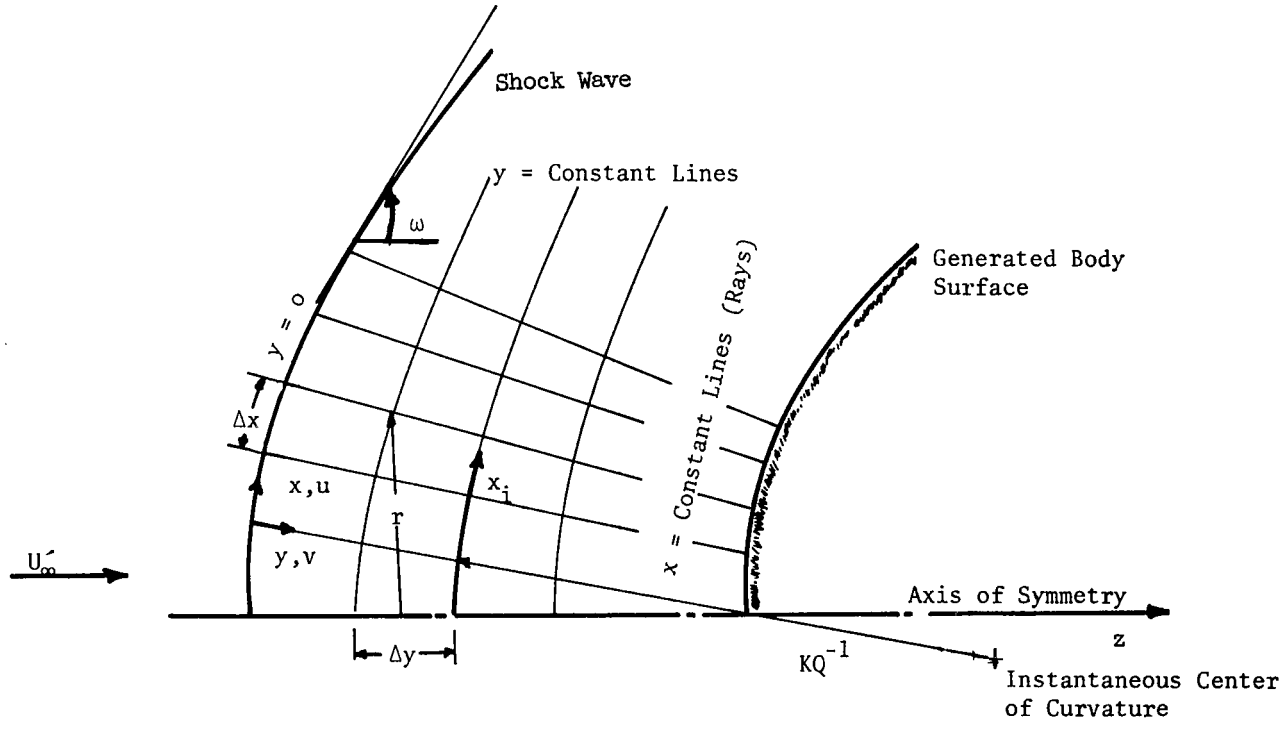

Figure 1.- Schematic of coordinate system and flow field.

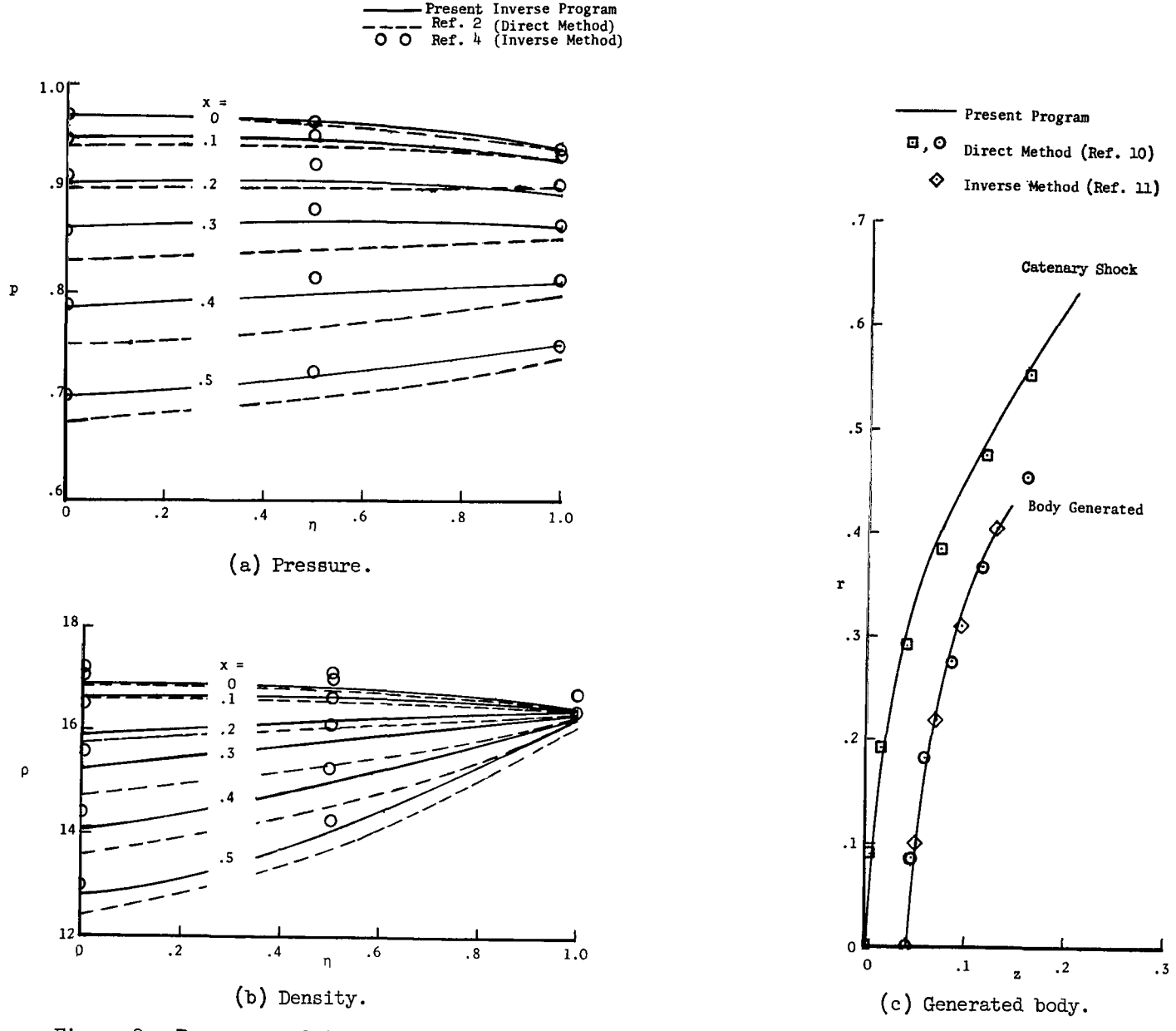

(a) Pressure.

(b) Density.

(c) Generated body.

Figure 2.- Pressure and density profiles and body coordinates from three different programs for nonradiating equilibrium air. U'_∞ = 13.72 km/sec; $\rho_\infty/\rho_{SL} = 2.57 \times 10^{-4}$.

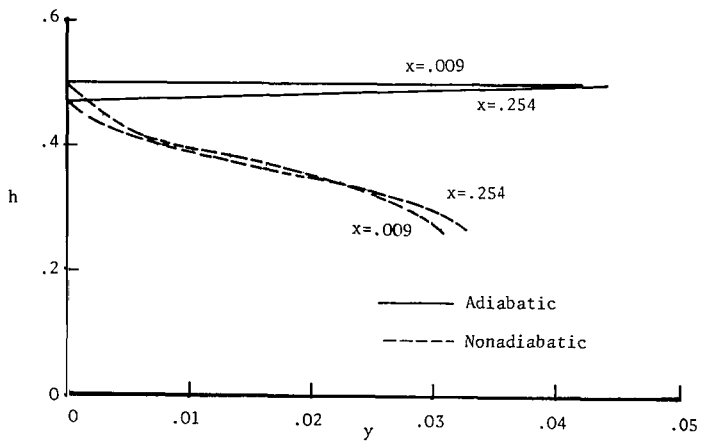

(a) Enthalpy.

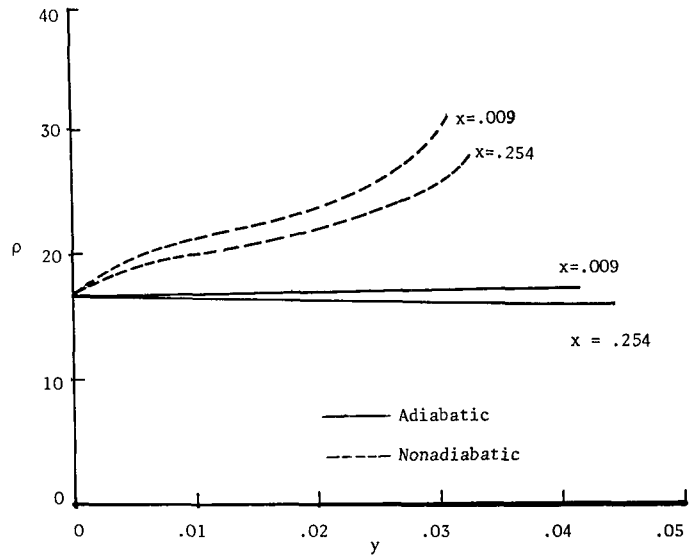

(b) Density.

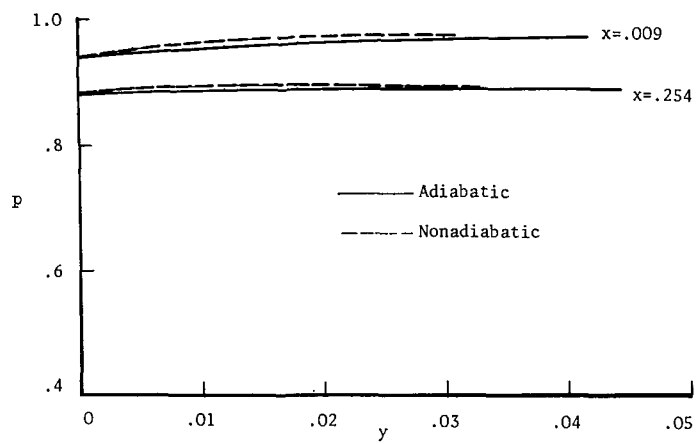

(c) Pressure.

Figure 3.- Flow parameter profiles for adiabatic and nonadiabatic conditions. $U_\infty' = 14.55$ km/sec; $\rho_\infty/\rho_{SL} = 1.84 \times 10^{-4}$; $R_b' = 343.80$ cm.

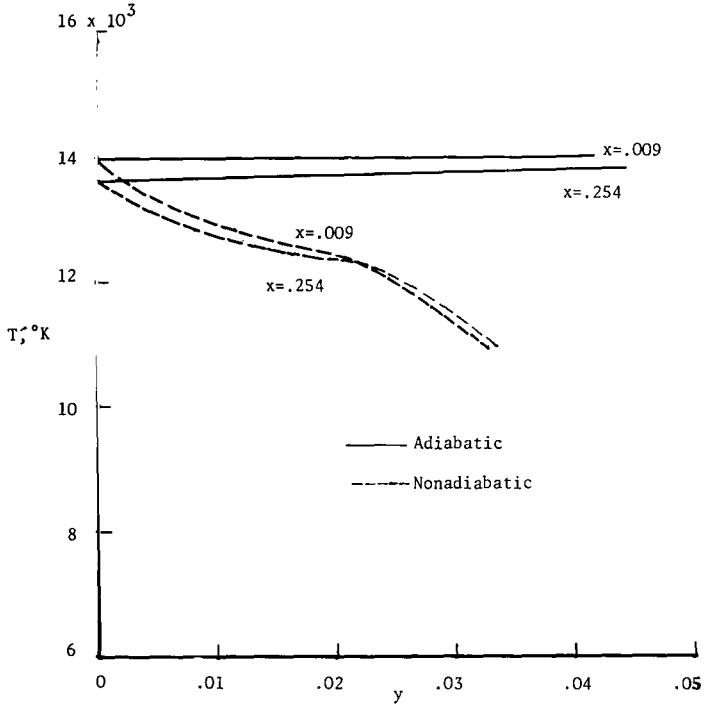

(d) Temperature.

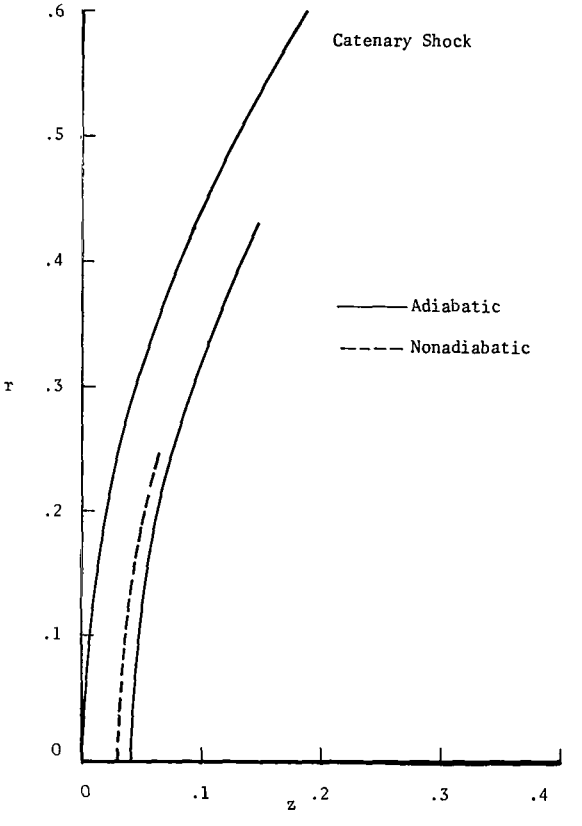

(e) Generated bodies for catenary shock shape.

Figure 3.- Concluded.

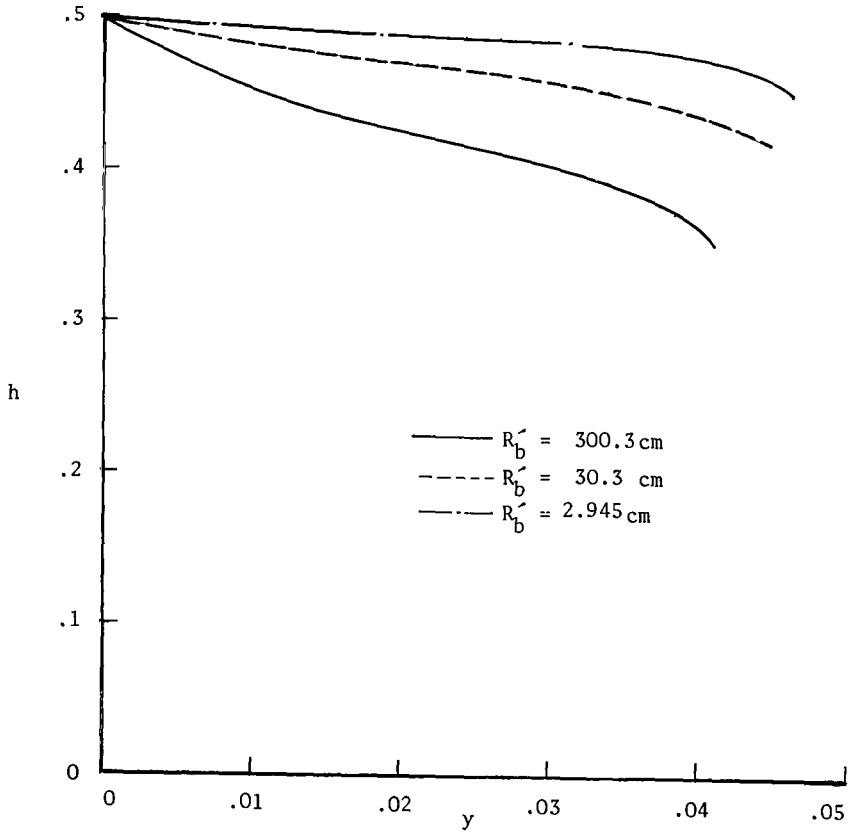

Figure 4.- Variation of stagnation-streamline enthalpy profile with R_b'. U_∞' = 11.59 km/sec; ρ_∞/ρ_{SL} = 1.392 × 10^{-2}; altitude = 30.5 km.

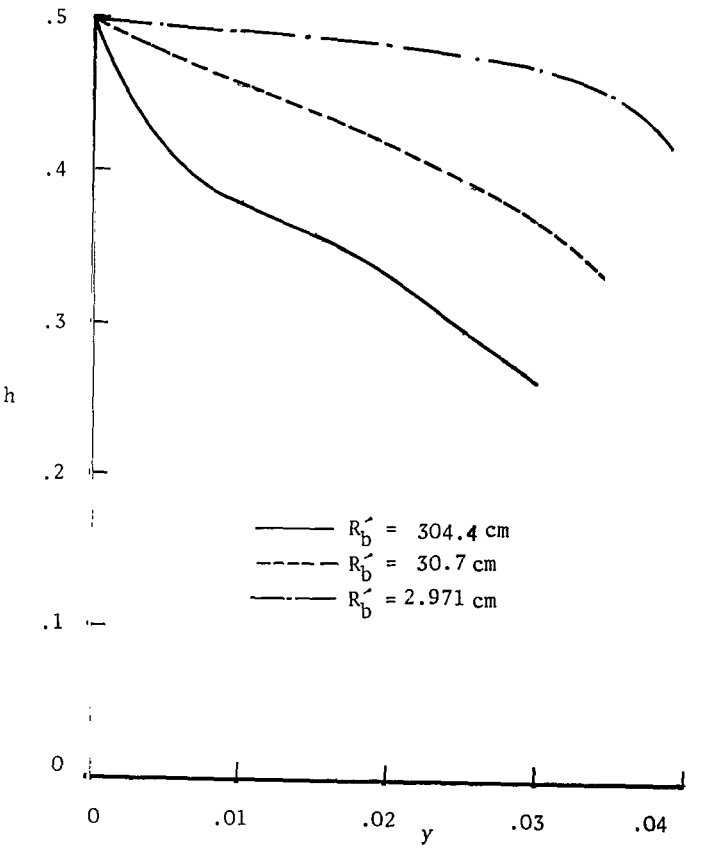

Figure 5.- Variation of stagnation-streamline enthalpy profile with R_b'. U_∞' = 15.25 km/sec; ρ_∞/ρ_{SL} = 2.2064 × 10^{-4}; altitude = 61.0 km.

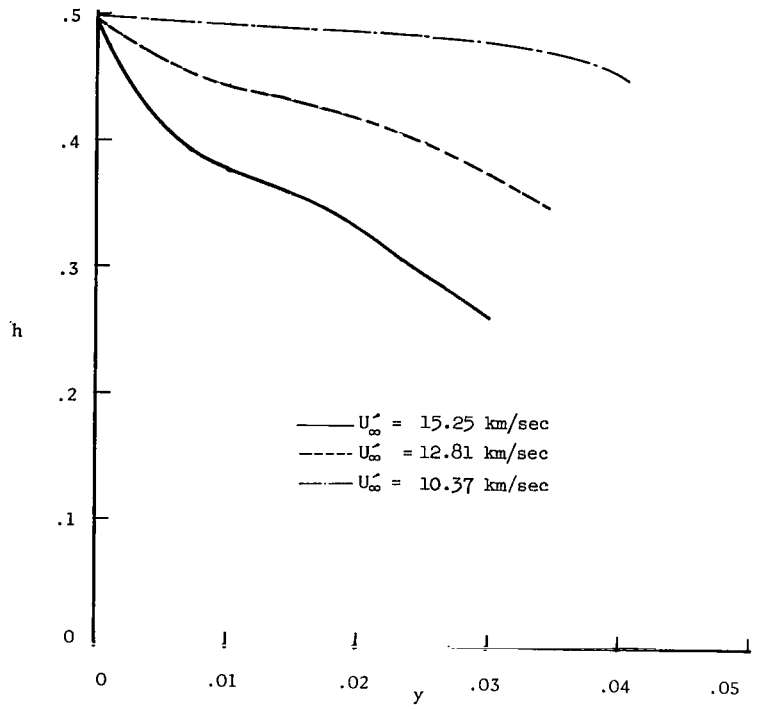

Figure 6.- Variation of stagnation-streamline enthalpy profile with U'_b. R'_b = 305 (reference value); $\rho_\infty/\rho_{SL} = 2.2064 \times 10^{-4}$; altitude = 61.0 km.

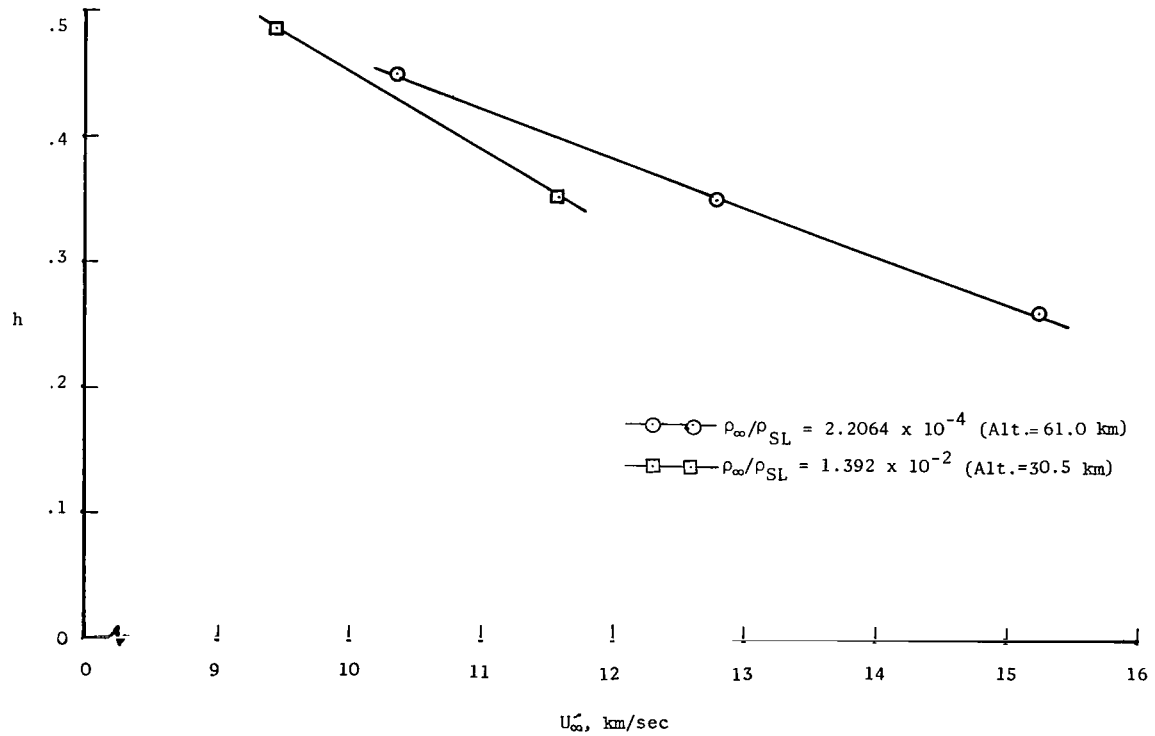

Figure 7.- Effect of free-stream density and velocity on stagnation-point enthalpy. R'_b = 305 cm (reference value).

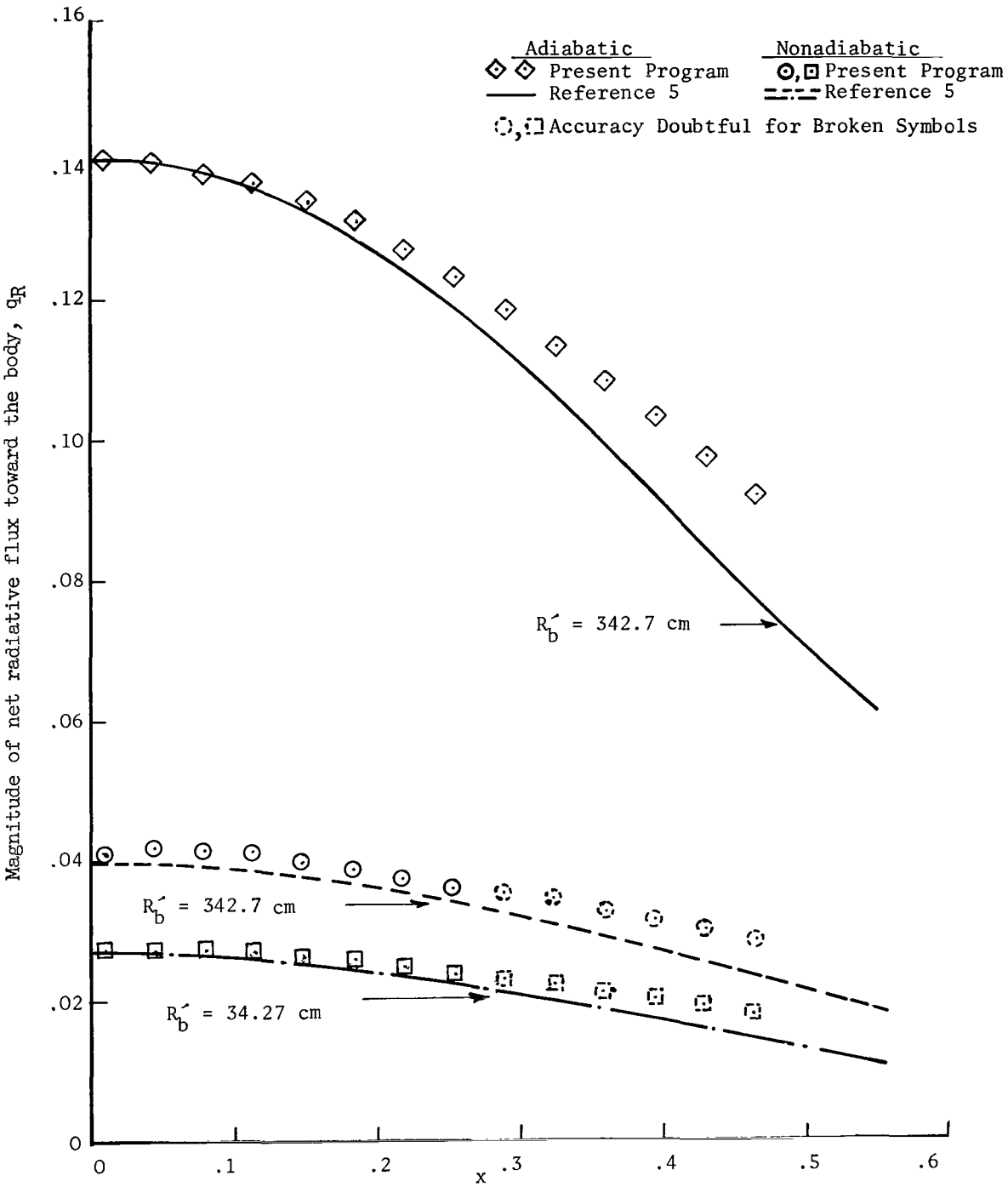

Figure 8.- Comparison of radiative heat flux along body surfaces from present inverse program with results from the direct method. U_∞' = 14.55 km/sec; $\rho_\infty/\rho_{SL} = 1.84 \times 10^{-4}$.

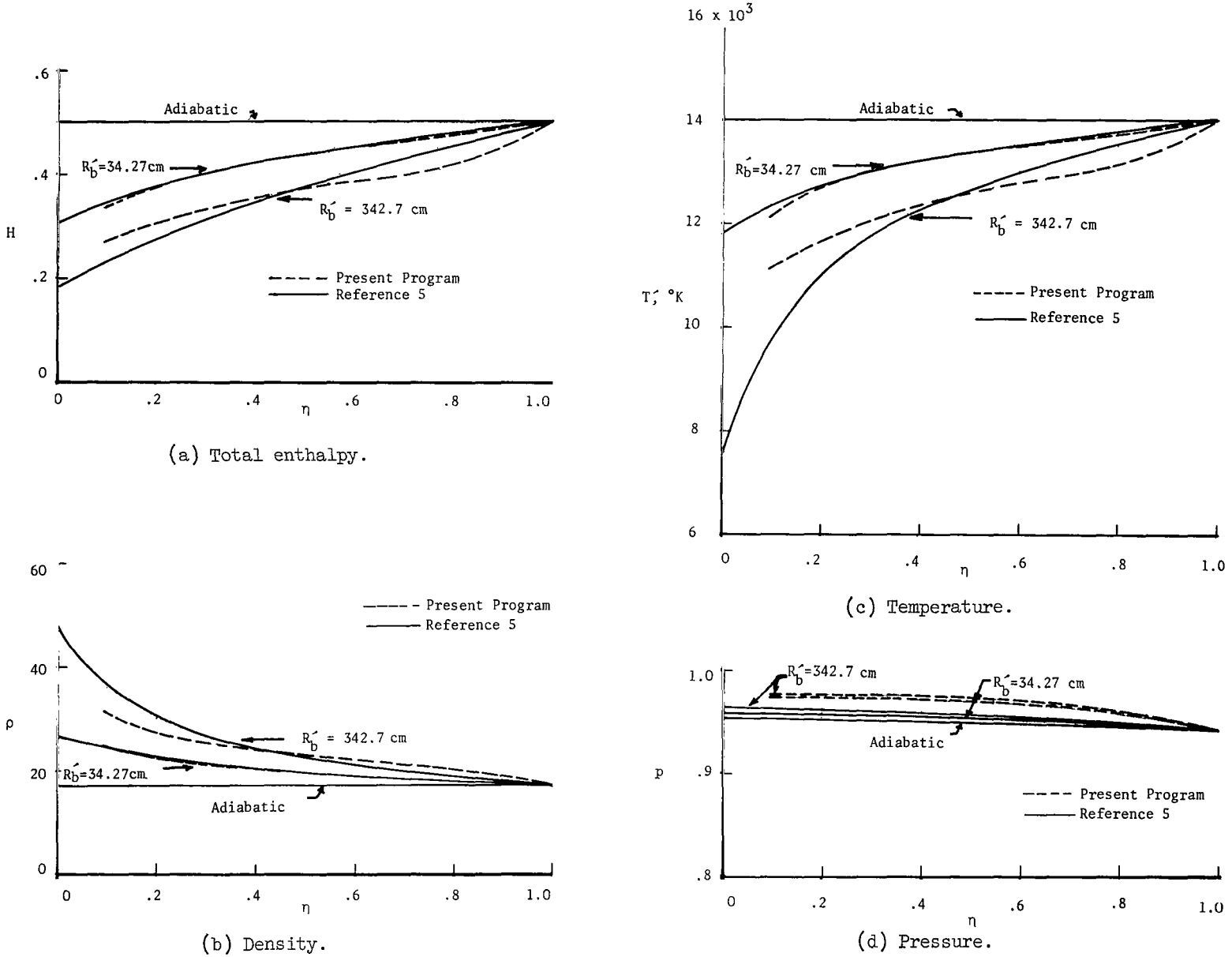

Figure 9.- Comparison of stagnation-streamline flow parameter profiles from the present inverse program with results from direct method. $U_\infty' = 14.55$ km/sec; $\rho_\infty/\rho_{SL} = 1.84 \times 10^{-4}$.

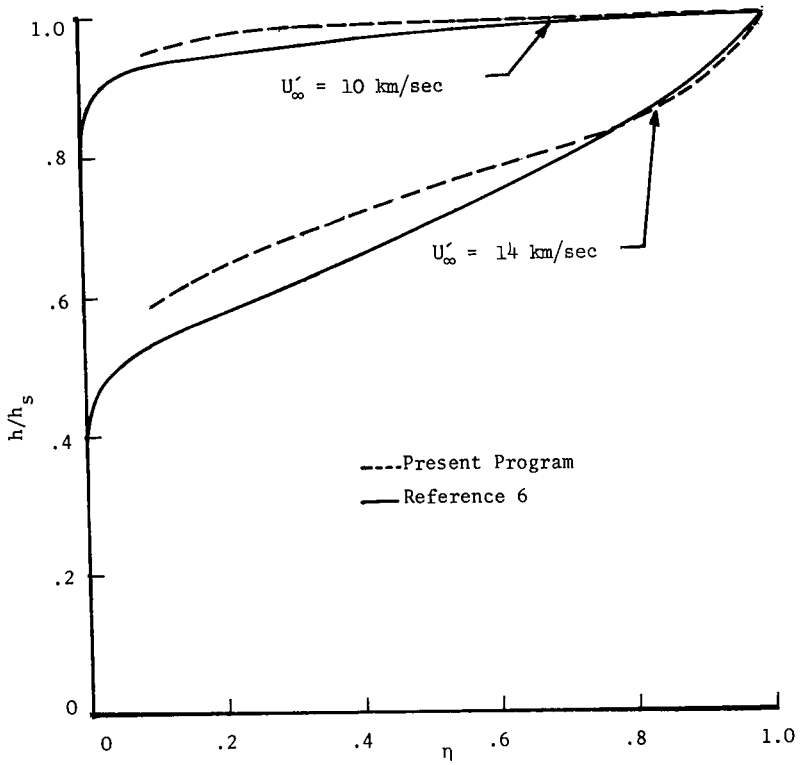

Figure 10.- Comparison of stagnation-streamline enthalpy profiles from inverse method with those from time-asymptotic method (reference 6). $\rho_\infty/\rho_{SL} = 10^{-3}$; $R_b' = 200$ cm (reference value).

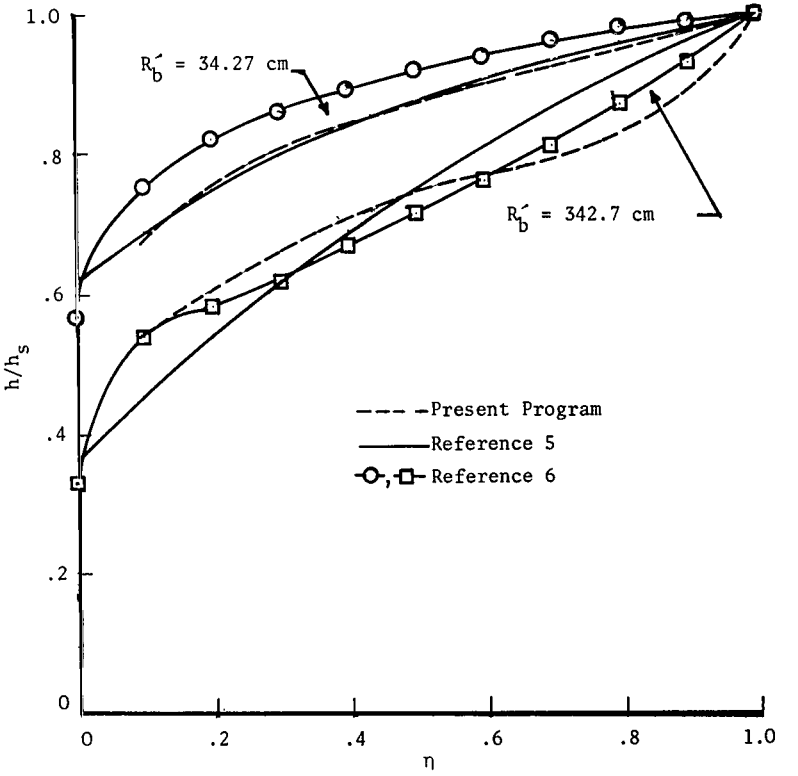

Figure 11.- Comparison of stagnation-streamline enthalpy profiles from present program with those from reference 5 and reference 6. $U_\infty' = 14.55$ km/sec; $\rho_\infty/\rho_{SL} = 1.84 \times 10^{-4}$.

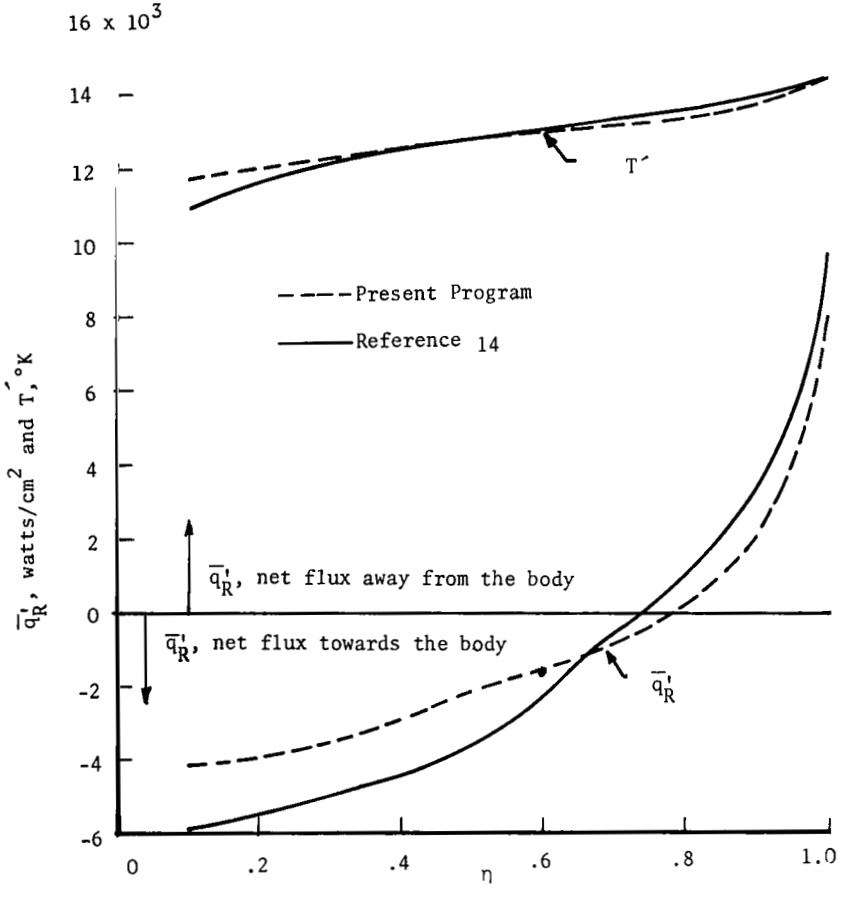

Figure 12.- Comparison of stagnation-streamline temperature and radiation heat-flux profiles from present inverse program with those from reference 14. U_∞' = 15.25 km/sec; ρ_∞/ρ_{SL} = 2.2064 x 10^{-4}; R_b' = 305 cm (reference value).

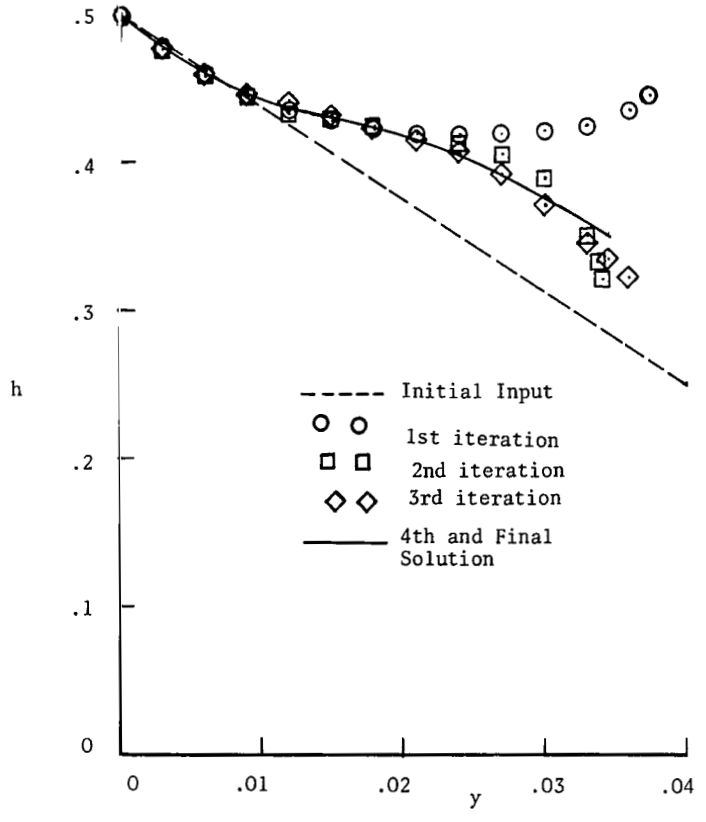

Figure 13.- Stagnation-streamline enthalpy profiles for each iterative solution including the final one. U_∞' = 12.81 km/sec; ρ_∞/ρ_{SL} = 2.2064 x 10^{-4}; R_b' = 305 cm (reference value); J = 9; 14 rays.

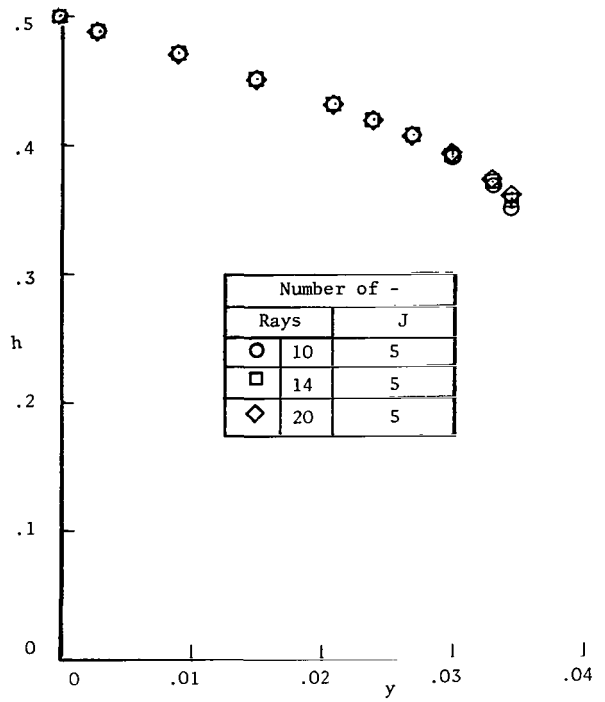

Figure 14.- Stagnation-streamline enthalpy profile with number of rays. $U_\infty' = 14.55$ km/sec; $\rho_\infty/\rho_{SL} = 1.84 \times 10^{-4}$; $R_b' = 34.44$ cm.

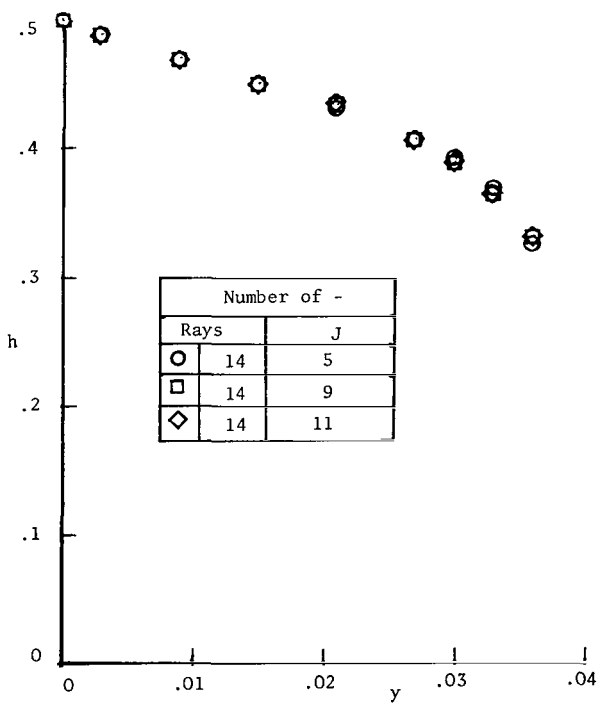

Figure 15.- Stagnation-streamline enthalpy profile with J. $U_\infty' = 14.55$ km/sec; $\rho_\infty/\rho_{SL} = 1.84 \times 10^{-4}$; $R_b' = 34.44$ cm.

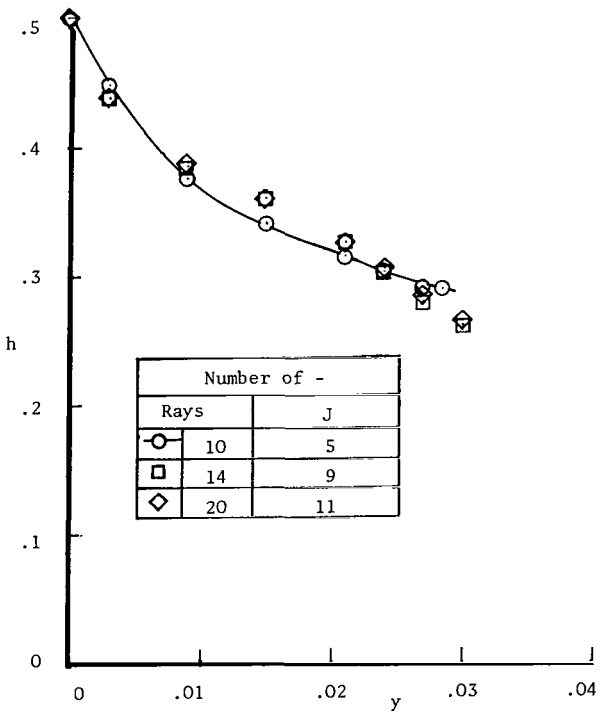

Figure 16.- Stagnation-streamline enthalpy profile with the number of rays and J. $U_\infty' = 15.25$ km/sec; $\rho_\infty/\rho_{SL} = 2.2064 \times 10^{-4}$; $R_b' = 305$ cm (reference value).

NASA-Langley, 1970 — 1 L-7209

01U 001 26 51 3DS 70212 00903
AIR FORCE WEAPONS LABORATORY /WLOL/
KIRTLAND AFB, NEW MEXICO 87117

ATT E. LOU BOWMAN, CHIEF,TECH. LIBRARY

"The aeronautical and space activities of the United States shall be conducted so as to contribute . . . to the expansion of human knowledge of phenomena in the atmosphere and space. The Administration shall provide for the widest practicable and appropriate dissemination of information concerning its activities and the results thereof."

—NATIONAL AERONAUTICS AND SPACE ACT OF 1958

NASA SCIENTIFIC AND TECHNICAL PUBLICATIONS

TECHNICAL REPORTS: Scientific and technical information considered important, complete, and a lasting contribution to existing knowledge.

TECHNICAL NOTES: Information less broad in scope but nevertheless of importance as a contribution to existing knowledge.

TECHNICAL MEMORANDUMS: Information receiving limited distribution because of preliminary data, security classification, or other reasons.

CONTRACTOR REPORTS: Scientific and technical information generated under a NASA contract or grant and considered an important contribution to existing knowledge.

TECHNICAL TRANSLATIONS: Information published in a foreign language considered to merit NASA distribution in English.

SPECIAL PUBLICATIONS: Information derived from or of value to NASA activities. Publications include conference proceedings, monographs, data compilations, handbooks, sourcebooks, and special bibliographies.

TECHNOLOGY UTILIZATION PUBLICATIONS: Information on technology used by NASA that may be of particular interest in commercial and other non-aerospace applications. Publications include Tech Briefs, Technology Utilization Reports and Notes, and Technology Surveys.

Details on the availability of these publications may be obtained from:

SCIENTIFIC AND TECHNICAL INFORMATION DIVISION

NATIONAL AERONAUTICS AND SPACE ADMINISTRATION

Washington, D.C. 20546